

General fringe decomposition and statistical bias correction in Optical Interferometry

Hrobjartur Thorsteinsson^a and David F. Buscher^a

^aUniversity of Cambridge, Cavendish Laboratory, Madingley Road, Cambridge, CB3 0HE, U.K.

ABSTRACT

Interferometric fringes are traditionally decomposed using the Discrete Fourier Transform (DFT). However, the application of the DFT is only correct in cases where the fringes are sampled evenly with delay and over integer number of fringe periods. This ideal case is often not achieved in Optical Interferometry. Fringe spectrography, non-linear fringe sweeps and image-plane beam combiners are typical cases of where the DFT approach fails to make most efficient use of the data. The authors assert that in many cases alternative and more efficient fringe decompositions exist but which may exhibit considerably different noise behaviour to the DFT. The authors present the mathematical results important for correcting for statistical bias in the powerspectrum and bispectrum constructs of a completely general fringe decomposition. An estimator for the noise in the powerspectrum has also been derived. The authors believe this to be the first analytical derivation of statistical bias and noise in interferometry that treats both photon counting noise as well as Gaussian read out noise.

Keywords: optical interferometry, fringe modulation, fringe decomposition, statistical bias, bias correction, read noise

1. INTRODUCTION

The aim of this paper is to introduce methods and results for fringe decomposition and statistical bias correction that are more applicable to realistic fringe measurements in interferometry. The original results for correcting Poisson bias in the powerspectrum and the bispectrum are due to Goodman^{1,2}, Belsher² and Wirnitzer.³ The analysis presented by these authors was originally based on speckle interferometry where the Discrete Fourier Transform (DFT) was taken as the best mean decomposition to the data set. In most optical interferometers today we deal with a small set of fringe components that may be unevenly sampled leading to the fringe defects depicted by the non-triangular fringe modulation in Fig.2. Fringes may also be recorded over non-integer fringes and/or the fringe composition functions may simply be non-sinusoidal such as in the case of an image plane beam combiner. The problem associated with applying the wrong decomposition to the fringe data results not only in incorrect fringe bias estimation, but also in spectral leakage or aliasing into neighbouring fringe frequencies.

The preliminary results that are presented in this publication are currently being prepared for a fully refereed journal article.

Further author information:

H.Thorsteinsson: E-mail: h.thorsteinsson@mrao.cam.ac.uk

D.Buscher: E-mail: d.buscher@mrao.cam.ac.uk

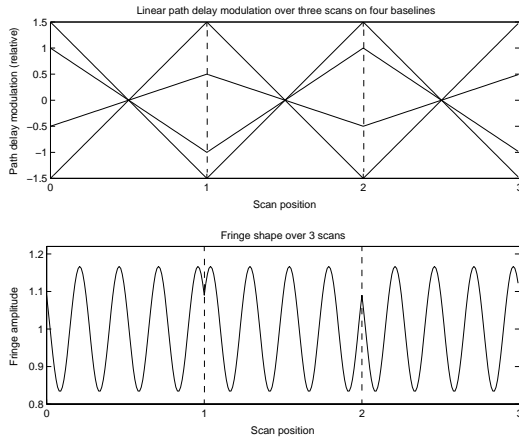


Figure 1: Linear 4-way modulation over integer number of fringes. The decomposition of the fringe amplitudes is achieved via the Discrete Fourier Transform.

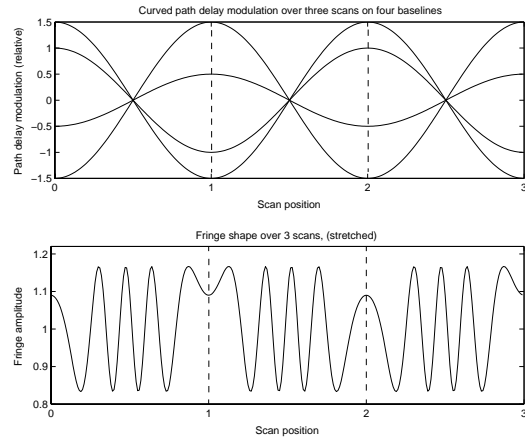


Figure 2: Curved 4-way modulation over integer number of fringes. This is an example of where the decomposition of the fringe amplitudes is achieved via some alternative transform.

2. GENERALISED FRINGE DECOMPOSITION

We will consider an instrument built for the purpose of inferring some property Γ_q of some underlying intensity distribution $\{\Lambda_p\}$ at the fringe detectors p . In Optical Interferometry the fringes may be expected to be roughly sinusoidal (pupil plane) or Gaborian (image plane) in shape. However, these analytical ideas of the fringe nature will never be strictly correct as fringes may not be recorded evenly with delay and the instrument may exhibit some unexpected features due to vignetting and/or other defects in the beam combining optics. We shall therefore consider that our underlying intensity distribution $\mathbf{\Lambda}$ is constructed via the matrix transformation

$$\mathbf{\Lambda}^{\{m\}} = \mathbf{W}^{\{m \times n\}} \mathbf{\Gamma}^{\{n\}}, \quad (1)$$

where $\mathbf{W} \in \mathbb{C}^{m \times n}$ is the matrix of any general wavelets appropriate for estimating the fringe amplitudes $\mathbf{\Gamma} \in \mathbb{C}^n$. These wavelets can be derived empirically from the interferometer and perhaps calibrated at the start of each observation session. In order to successfully invert this linear system we require that the dimension of $\mathbf{\Lambda} \in \mathbb{R}^m$ be at least twice that of $\mathbf{\Gamma}$. Actually, we do a little better than this as we require to decompose the zero frequency component of the fringe signal which has no imaginary part. Hence, we can solve for the fringe amplitudes given that $m \geq 2n - 1$. From a general point of view our fringe decomposition shall be over-determined and so we must choose a pseudo-inverse from an infinite selection of suitable inverses to equation (1). The most obvious choice of inverse is the one correct in the least-squares sense. It is also the inverse which, given the sinusoidal wavelet condition over integer period fringes, is equivalent to the DFT. The least-squares inverse is also known as the Moore-Penrose (MP) inverse and can be shown to be the solution to the system

$$(\mathbf{W}^\dagger \mathbf{W}) \mathbf{\Gamma} = \mathbf{W}^\dagger \mathbf{\Lambda}, \quad (2)$$

where the suffix \dagger denotes the Hermitian transpose of the matrix. The matrix inverse that will perform the fringe decomposition is then

$$\mathbf{\Gamma} = \mathbf{H} \mathbf{\Lambda},$$

where

$$\mathbf{H} = (\mathbf{W}^\dagger \mathbf{W})^{-1} \mathbf{W}^\dagger, \quad \mathbf{H} \in \mathbb{C}^{n \times m}. \quad (3)$$

Least squares matrix inversion is well documented in the literature⁴ and is most popularly obtained via the Singular Value Decomposition or the Householder triangularisation of \mathbf{W} .

3. NOISE MODEL

When applied to the real data \mathbf{L} , statistical bias will occur in many cases for non-linear constructs of the fringe decomposition

$$G_m = \sum_n L_n H_{mn}. \quad (4)$$

The fringe data is the underlying intensity distribution embedded in noise associated with photon counting statistics as well as instrument detector gain errors. Phase and intensity fluctuations due to atmospheric turbulence and variation in internal alignment of the instrumentation are also a source of noise on the fringe data. This type of noise is normally ill understood at the time of fringe integration but is assumed to change slowly enough so to allow for calibration on a well known reference star. In our analysis we will avoid making assumptions on the behaviour of any statistics of badly predictable nature but leave open the possibility for further analysis of such noise as it may become better understood in the future.

We decide to model our understood noise as being of photon counting nature but convolved with a fixed Gaussian detector noise. The probability distribution of our detector providing a gain of L is therefore

$$P(L|\Lambda, \sigma) = \int_0^L P_P(N|\Lambda) P_G(N-L|\sigma) dN, \quad (5)$$

where P_G and P_P are the Gaussian and Poisson probabilities respectively and N is the incident number of photons. Direct evaluation of the integral in equation (5) is unnecessary as for our following analysis we will solely be interested in the integer moments of this distribution. We invoke the convolution theorem⁵ which applies to the moment generating functions, M_G and M_P of P_G and P_P . By convolution we may assert that the moment generating function of the probability density model is given by the multiplication,

$$M(\nu) = M_G(\nu) M_P(\nu) = e^{\frac{1}{2}\sigma^2\nu^2} \cdot e^{-\Lambda + \Lambda e^\nu}. \quad (6)$$

We can now evaluate the required moments for the statistics. We require the first four moments to derive the results to follow. These are

$$E(L) = \frac{dM}{d\nu}(0) = \Lambda, \quad (7)$$

$$E(L^2) = \frac{d^2M}{d\nu^2}(0) = \Lambda^2 + \Lambda + \sigma^2, \quad (8)$$

$$E(L^3) = \frac{d^3M}{d\nu^3}(0) = \Lambda^3 + 3\Lambda^2 + \Lambda + 3\Lambda\sigma^2 \quad \text{and} \quad (9)$$

$$E(L^4) = \frac{d^4M}{d\nu^4}(0) = \Lambda^4 + 6\Lambda^3 + 7\Lambda^2 + \Lambda + 6\Lambda^2\sigma^2 + 6\Lambda\sigma^2 + 3\sigma^4. \quad (10)$$

On inspecting this result we see that our model yields not only the individual moments of the Poisson and Gaussian distributions, but in addition we have the cross terms $\Lambda\sigma^2$ and $\Lambda^2\sigma^2$. Bias and noise from the detector statistics are most significant at low light levels and the cross terms are most significant in the region where $\Lambda \sim \sigma$ or close to the likely limiting sensitivity of an interferometer. Finally, we also note that any two different realisations of our noise model will be stochastically independent,

$$E(L_p^a L_q^b) = E(L_p^a)E(L_q^b). \quad (11)$$

4. POWERSPECTRUM BIAS

The powerspectrum is an important estimator for the amplitude of fringes in interferometry. The powerspectrum estimator is applied for incoherent averaging of the fringe frames where typically individual fringe integrations are at low light levels and statistical bias will be significant. Following the derivation procedure in Appendix A we have derived the unbiased powerspectrum estimator as follows.

$$\Gamma_m \Gamma_m^* = E(G_m G_m^* - P_m^{(1)}) - \Sigma_m^{(1)}, \quad (12)$$

where we define the two new transforms $P_m^{(1)}$ and $\Sigma_m^{(1)}$ (Appendix C) due to the Poisson and Gaussian detector noise respectively. We label these transforms with the index (1) due their popular appearance with other variations in the bispectrum bias and powerspectrum variance. It is clear from the construction of $P_m^{(1)}$, that if the transformation matrix happens to be the DFT, $H_{mn} = e^{i2\pi mn}$, then the bias becomes the total photon flux in the integration \mathbf{L} . This is in agreement with the results demonstrated by Goodman¹² & Belsher,²

$$\Gamma_m \Gamma_m^* = E(G_m G_m^* - G_0). \quad (13)$$

The result for the variance of the bias corrected bispectrum has been derived and is presented in Appendix B.

5. BISPECTRUM BIAS

The bispectrum construct is the estimator user for applying phase constraints to fringe amplitude measurements in optical interferometry and is critical to complex synthesis imaging. The statistical bias in the bispectrum has been derived in a similar fashion to the powerspectrum bias.

$$\begin{aligned} \Gamma_a \Gamma_b \Gamma_c^* &= E(G_a G_b G_c^* \\ &\quad - P_{b,c}^{(1)} G_a - P_{a,c}^{(1)} G_b - P_{a,b}^{(2)} G_c^* \\ &\quad - \Sigma_{b,c}^{(1)} G_a - \Sigma_{a,c}^{(1)} G_b - \Sigma_{a,b}^{(2)} G_c^* \\ &\quad + 2P_{a,b,c}^{(3)}). \end{aligned} \quad (14)$$

The equivalent result due to Wirnitzer³ in case of the DFT condition is

$$\begin{aligned} \Gamma_a \Gamma_b \Gamma_c^* &= E(G_a G_b G_c^* \\ &\quad - G_a^* G_a - G_b^* G_b - G_c^{(2)} G_c^* \\ &\quad + 2G_0) \end{aligned} \quad (15)$$

As required, the general bias correction in equation (14) does indeed reduce to the Wirnitzer³ result when substituting the DFT transform, $H_{mn} = e^{i2\pi mn}$. One consequence of equation (14) is that bias will now both effect the real part and imaginary part of the bispectrum depending on the property of the fringe decomposition.

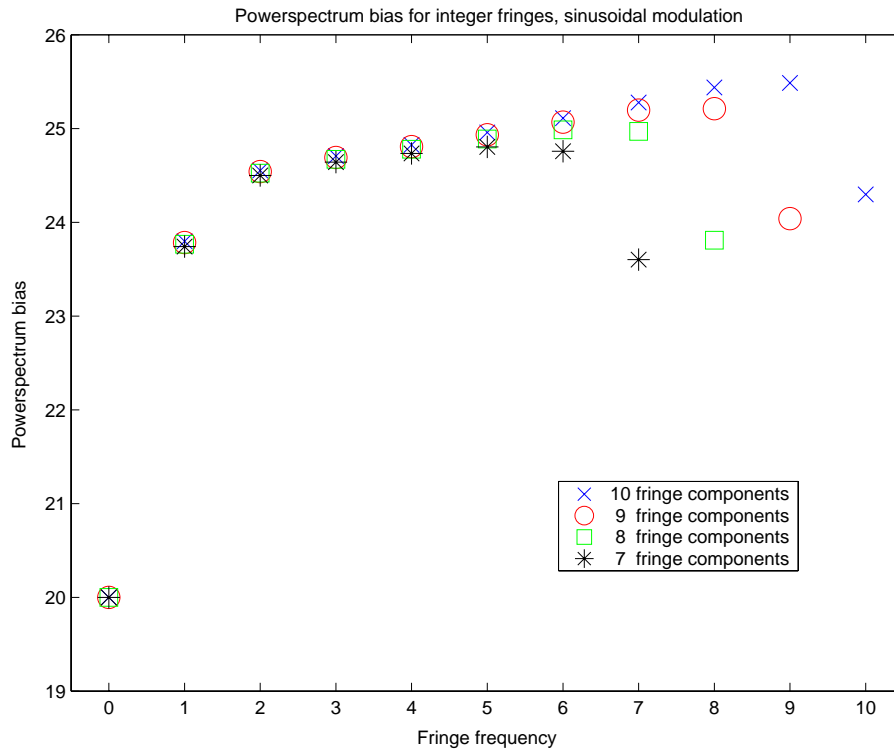


Figure 3: Sinusoidal fringe modulation over integer number of fringes as demonstrated in Fig. 2. Bias varies with frequency and phase of the underlying fringe.

6. VARIOUS RESULTS

6.1. Powerspectrum bias

We have modelled a pupil plane all-in-one beam combiner and calculated the bispectrum bias at 10 photon counts per beam combiner output. A sinusoidal fringe modulation is assumed resulting in non-evenly sampled fringes and a non-orthogonal fringe decomposition. Two complimentary outputs from the beam combiner are analysed as a pair bringing the total fringe flux to 20 photons per sweep. The complimentary outputs are the two existing outputs which add to give a constant underlying fringe flux. This approach has the effect of improving the orthogonality and noise behaviour of the fringe decomposition. In Fig. 3 the powerspectrum bias is plotted against fringe frequency for fringes containing a number of different fringe components all at visibilities equal to 1 and at zero phase. It is clear that the bias varies with frequency and rises above the constant bias obtained with linear, integer fringe sampling.

6.2. SNR in fringe sampling

We model the same type of beam combiner and data analysis as in section 6.1, but plot the SNR against the number of integration bins assuming three fringe components. Two types of modulations are compared, the triangular modulation as in Fig. 1 and the sinusoidal modulation as in Fig. 2. In Fig. 4 we see how the signal rises rapidly from zero after the decomposition becomes well conditioned at $(2 \times 4) - 1 = 7$ bins. The non-orthogonal fringe decomposition appears

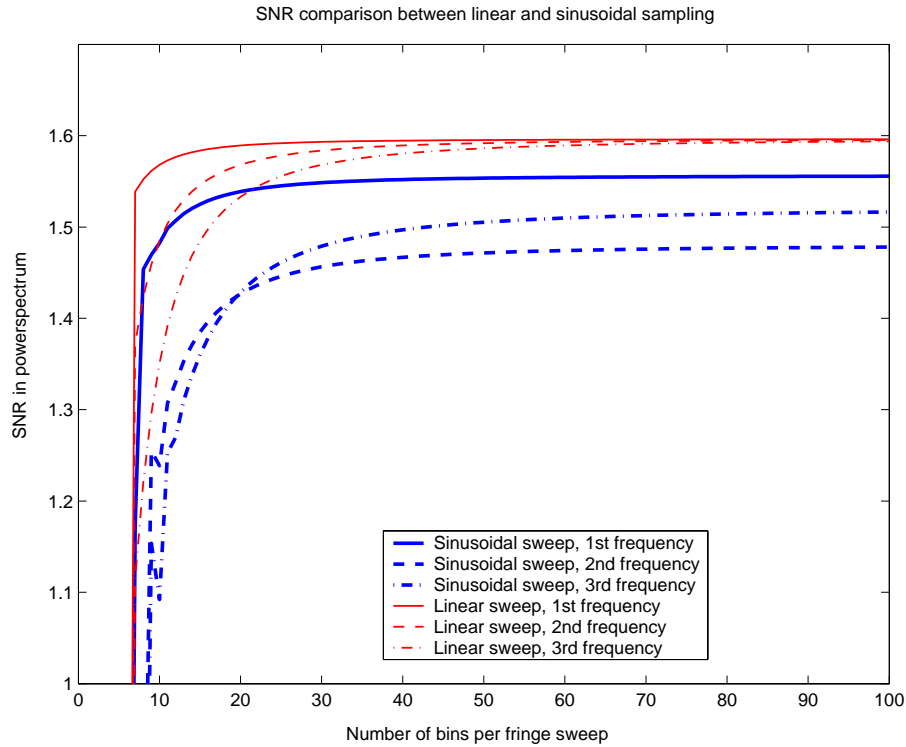


Figure 4: Linear and sinusoidal fringe modulation. Peak SNR for sinusoidal modulation depends on both frequency and phase but is not significantly lower than in the linear modulation case.

to have a well behaved noise property and peaks on average at ca. 5% below the orthogonal DFT case.

6.3. SNR in fringe spectrography

We have modelled spectrally dispersed, evenly lit and linearly sample fringes as might be obtained using a pupil plane beam combiner and a fringe spectrograph. Two methods of fringe analysis are compared. The first approach is a non-orthogonal decomposition that takes account of all the fringe flux in the spectral channels and in the second approach we taper the spectral channels down to integer fringes and then decompose using the DFT. In Fig. 5 it is clear that greater SNR efficiency is achieved when using the non-orthogonal decomposition approach. The non-orthogonal approach, due to its phase sensitivity, is optimised at different fringe phases for different spectral channels.

6.4. Bispectrum phase bias (AMBER)

We have investigated how the bispectrum bias differs for a typical image plane beam combiner when applying the traditional Wirnitzer³ bias correction in equation (15) and the actual fringe bias given by equation (14). The fringes have been modelled based on AMBER specifications kindly provided by Sylvie Robbe-Dubois and the article in the 2002 SPIE proceedings.⁶ In Fig. 6 we have plotted the closure phase bias due to Poisson noise for 10, 17 and 30 photons per integration on the CCD.

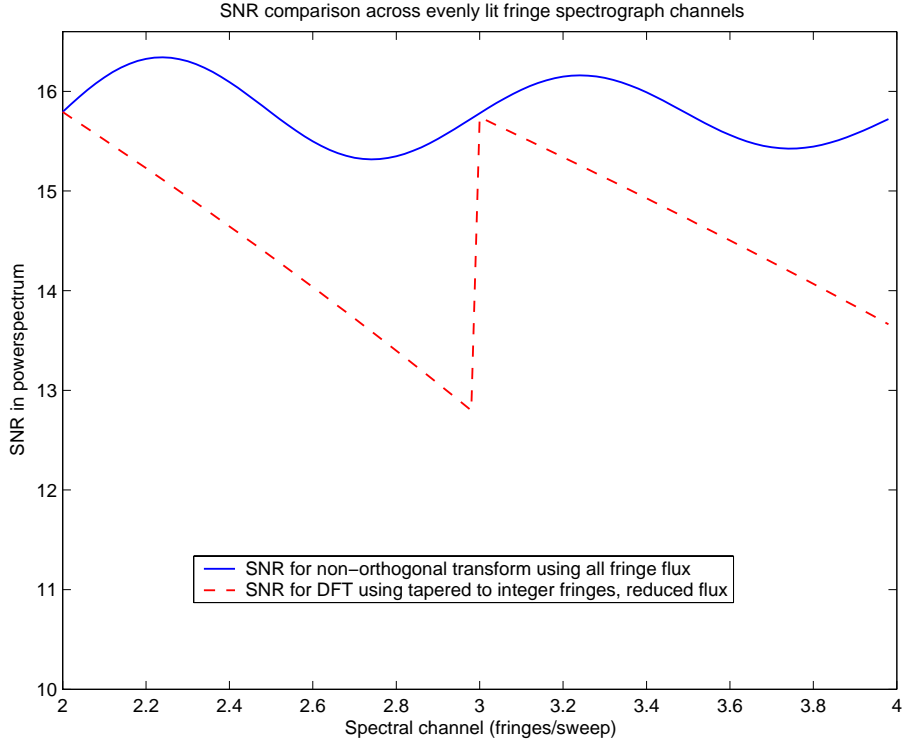


Figure 5: Spectrally dispersed, evenly lit, linearly sampled fringes. Non-orthogonal and orthogonal fringe decompositions are compared.

APPENDIX A. BIAS CORRECTED POWERSPECTRUM DERIVATION

$$\begin{aligned}
 E(G_m G_m^*) &= \sum_k \sum_l E(L_k L_l) H_{ml} H_{mk}^* \\
 &= \sum_{k \neq l} \sum_l E(L_k) E(L_l) H_{ml} H_{mk}^* + \sum_q E(L_q^2) H_{mq} H_{mq}^*
 \end{aligned}$$

and expanding the moments using equations (7-10) we get

$$\begin{aligned}
 &= \sum_{k \neq l} \sum_l \Lambda_k \Lambda_l H_{mk} H_{ml}^* + \sum_q \Lambda_q^2 H_{mq} H_{mq}^* + \sum_q \Lambda_q H_{mq} H_{mq}^* + \sum_q \sigma_q^2 H_{mq} H_{mq}^* \\
 &= \Gamma_m \Gamma_m^* + E \left(\sum_q L_q H_{mq} H_{mq}^* \right) + \sum_q \sigma_q^2 H_{mq} H_{mq}^*.
 \end{aligned}$$

We have therefore constructed the bias corrected estimator as

$$\Gamma_m \Gamma_m^* = E \left(G_m G_m^* - P_m^{(1)} \right) - \Sigma_m^{(1)}$$

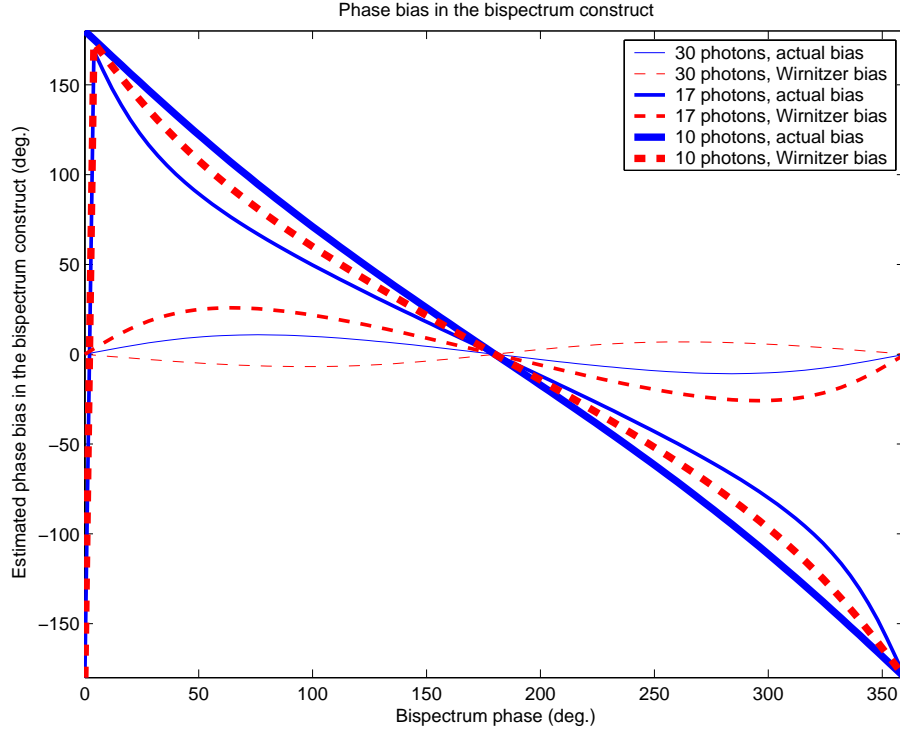


Figure 6: Comparison of the actual bispectrum bias and the Wirnitzer³ bias in phase. The graphs shows how at low light levels the Wirnitzer bias correction when applied to AMBER data may often result in very unreliable phase estimates.

APPENDIX B. POWERSPECTRUM VARIANCE

$$\begin{aligned}
 \sigma^2 &= E \left((GG^* - P^{(1)} - \Sigma^{(1)})^2 \right) - (\Gamma\Gamma^*)^2 \\
 &= \\
 &\textbf{Poisson terms:} \\
 &+ (\Phi^{(1)})^2 + 2\Phi^{(1)}\Gamma\Gamma^* + \Phi^{(2)}\Phi^{(2)*} \\
 &+ (\Phi^{(2)}\Gamma^*\Gamma^* + \Phi^{(2)*}\Gamma\Gamma) \\
 &\textbf{Gaussian terms:} \\
 &+ (\Sigma^{(1)})^2 + 2\Sigma^{(1)}\Gamma\Gamma^* + \Sigma^{(2)}\Sigma^{(2)*} \\
 &+ (\Sigma^{(2)*}\Gamma\Gamma + \Sigma^{(2)}\Gamma^*\Gamma^*) \\
 &+ \Sigma^{(4)} - 2(\Sigma^{(3)}\Gamma^* + \Sigma^{(3)*}\Gamma) \\
 &\textbf{Gaussian-Poisson coupled terms:} \\
 &+ 2\Sigma^{(1)}\Phi^{(1)} \\
 &+ (\Sigma^{(2)*}\Phi^{(2)} + \Sigma^{(2)}\Phi^{(2)*})
 \end{aligned}$$

APPENDIX C. ADDITIONAL TRANSFORM DEFINITIONS

$$\begin{aligned}
 P_{a,b}^{(1)} &= \sum L_q(H_{a,q}H_{b,q}^*) & E(P_{a,b}^{(1)}) &= \Phi_{a,b}^{(1)} \\
 P_{a,b}^{(2)} &= \sum L_q(H_{a,q}H_{b,q}) & E(P_{a,b}^{(2)}) &= \Phi_{a,b}^{(2)} \\
 P_{a,b,c}^{(3)} &= \sum L_q(H_{a,q}H_{b,q}H_{c,q}^*) & E(P_{a,b,c}^{(3)}) &= \Phi_{a,b,c}^{(3)} \\
 \Sigma_{a,b}^{(1)} &= \sum \sigma_q^2(H_{a,q}H_{b,q}^*) & \Sigma_{a,b}^{(2)} &= \sum \sigma_q^2(H_{a,q}H_{b,q}) \\
 \Sigma_{a,b,c}^{(3)} &= \sum \sigma_q^2(H_{a,q}H_{b,q}H_{c,q}^*) & \Sigma_{a,b,c,d}^{(4)} &= \sum \sigma_q^2(H_{a,q}H_{b,q}^*H_{c,q}H_{d,q}^*)
 \end{aligned}$$

REFERENCES

1. J. Goodman, *Statistical Optics*, Wiley, New York, 1985.
2. J. Goodman and J. Belsher in *S.P.I.E Sminar Proc.*, **75**, p. 141, 1976.
3. B. Wirnitzer, "Bispectral analysis at low light levels and astronomical speckle masking," *Optical Society of America Journal* **2**, pp. 14–21, Jan. 1985.
4. L. Trefethen and D. Bau, *Numerical Linear Algebra*, Society for Industrial and Applied Mathematics, Philadelphia, 1997.
5. M. Bulmer, *Principles of Statistics*, Dover Publications, Inc., 1979.
6. G. Duvert, D. Mouillet, F. Malbet, P. Berio, T. Forveille, E. Aristidi, K. Hofmann, and P. Mege, "AMBER data simulator," in *Proc. SPIE Vol. 4006, p. 217-223, Interferometry in Optical Astronomy, Pierre J. Lena; Andreas Quirrenbach; Eds.*, pp. 217–223, July 2000.